Phase Equilibria and Thermodynamics of the Mg-Si-Li System and Remodeling of the Mg-Si System

D. Kevorkov, R. Schmid-Fetzer, and F. Zhang

(Submitted 8 June 2003)

The ternary Li-Mg-Si phase relations were established using high-purity samples prepared by levitation melting. Analysis was done using x-ray powder diffraction (XRD), optical metallography, and differential thermal analysis (DTA) in customized sealed tantalum crucibles. Three ternary intermetallic phases were confirmed in this system: τ_1 (Li$_8$MgSi$_6$), τ_2 (Li$_{12}$Mg$_3$Si$_4$), and τ_3 (Li$_2$MgSi). The LiMg$_2$Si phase reported previously is not a separate phase but the interstitial solid solution of Li in the binary Mg$_2$Si phase, Li$_x$Mg$_2$Si, at the maximum $x \approx 0.91 \pm 0.05$. Ternary liquidus data and phase transformations were also measured. A thermodynamic assessment of the ternary Li-Mg-Si system was worked out in parallel to the experimental study and used to select the relatively small number of our key experiments. The final consistent thermodynamic description is well supported by the present experimental data. It was found that the published thermodynamic parameter sets for the binary Mg-Si subsystem produce an artificial inverted liquid miscibility gap at higher temperatures. This system was remodeled to obtain data that could be reliably extrapolated to various temperatures and the ternary system. The experimentally supported calculated phase equilibria in the entire composition and temperature range of the Li-Mg-Si system are presented, including the liquidus surface and invariant reactions. Gradual changes in a monovariant eutectic/peritectic reaction type occur in this system. The intricacies involved due to solid solutions and the failure of the classic tangent criterion are discussed for some ternary alloys.

1. Introduction

The search for new magnesium (Mg) alloys is primarily driven by the demand for further weight reduction in automotive industry. Present Mg die casting alloys are based on the Mg-Al system. To achieve a better creep resistance, the Mg-Al based alloys should usually have a low Al-content and show the formation of stable intermetallic particles. A well-known alloying addition is silicon. Commercial Mg-Al-Si die casting alloys as AS41 and AS21 show improved creep resistance. On the other hand, in researched Mg-Al-Li alloys, Li addition produces a further density reduction and increases ductility. Small amounts of Li (<4 wt.%) also increase the corrosion resistance. The interactions of both alloying elements in the quaternary Mg-Al-Li-Si system are not known. For a focused development of new alloys in that system, the phase equilibria are needed together with the underlying thermodynamic data. The tool of computational thermodynamics can be used for such focused development through use of relevant thermodynamic data; such an approach has already been demonstrated for the development of other new Mg alloys [2001Sch]. The consistent generation of these data using both experimental work and thermodynamic calculations was the global aim of this work.

This study was done in the framework of the generation of a multicomponent database for Mg alloys. The ternary Li-Mg-Si system is also needed as an important subsystem for Mg-Li-Al-Si-X alloys. Since published experimental data about the Li-Mg-Si system are very limited, a particular experimental investigation was carried out in parallel with the thermodynamic modeling in this work. This procedure allowed the ternary key samples to be selected. Scrutinizing the published binary thermodynamic data sets resulted in the need to remodel the binary Mg-Si subsystem since an artificial inverted liquid miscibility gap at higher temperature was detected. The comprehensive comparison of the experimental Mg-Si data with the calculation from the new model is also presented in this work.

2. Literature Data

2.1 Ternary Constitutional Data

The few experimental investigations of the Li-Mg-Si system published in literature [1986Nes, 1992Pav1, 1992Pav2] presented altogether five ternary phases of various compositions. The isothermal section of the phase diagram at 200 °C was studied by [1992Pav2]. They prepared alloys by arc melting in a purified Ar atmosphere using a Li-Mg master alloy [1992Pav2]. Pure metals were also used for the preparation of alloys with a purity Li-98.2 wt.%, Mg-99.98 wt.%, and Si-99.9999 wt.%. Annealing was carried out in Ta containers at 200 °C for 240 h. X-ray powder diffraction (XRD) was used for the phase analysis. Four ternary phases Li$_5$MgSi$_4$, Li$_{12}$Mg$_3$Si$_4$, Li$_2$MgSi, and LiMg$_2$Si were reported in this system [1992Pav2]. All the

D. Kevorkov and R. **Schmid-Fetzer,** Technical University of Clausthal, Institute of Metallurgy, Robert-Koch-Str. 42 D-38678 Clausthal-Zellerfeld, Germany; and **F. Zhang,** Computherm, LLC, 437 S. Yellowstone Dr., Suite 217, Madison, WI 53719. Contact e-mail: Schmid-fetzer@tu-clausthal.de.
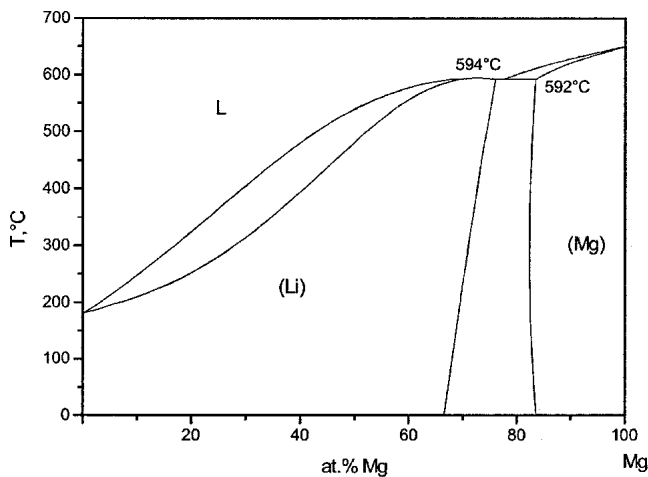
Fig. 1 Calculated phase diagram of the Li-Mg system using parameters of [1990Sau]

Fig. 2 Calculated phase diagram of the Li-Si system using parameters of [1995Bra]

phases have no significant solubility. In addition, no ternary solubility of binary phases was reported.

The crystal structures of three of the four phases were determined by XRD. The crystal structure of the Li_5MgSi_4 phase was not determined. Earlier [1986Nes] reported the monoclinic phase Li_8MgSi_6 ($Li_{53.33}Mg_{6.77}Si_{40}$), which has similar composition to Li_5MgSi_4 ($Li_{50}Mg_{10}Si_{40}$). It may be assumed that both compositions describe the same phase and Li_8MgSi_6 is the real composition of the phase. It will be shown later that the phase $LiMg_2Si$ actually corresponds to the solution phase Li_xMg_2Si extending from binary Mg_2Si.

2.2 Thermodynamics of Binary Systems Li-Mg and Li-Si

No thermodynamic data for the ternary Li-Mg-Si system could be found in literature. The parameter sets for the binary subsystems given in the literature are discussed below.

The thermodynamic model for the Li-Mg system is taken from the evaluation of Saunders presented in COST 507 database [1998Sau] (Fig. 1). These data were also presented in [1990Sau]. Differential thermal analysis (DTA) investigations, activity, and enthalpy measurements of the liquid phase were used for the optimization. The calculated phase diagram shows an excellent agreement with literature data. A detailed discussion and comparison with experimental data is presented in [1990Sau].

Two sets of parameters were published for the binary Li-Si system [1995Bra]. In the first assessment of [1995Bra] the chemical potential values for the solid two-phase regions are in good agreement with the experimental values. However, the liquidus in the region of the $Li_{12}Si_7$ and Li_7Si_3 phases shows significant deviation from the experimental points using the same partial Gibbs energies. In the second assessment, these potential values were neglected [1995Bra]. A better agreement with the experimental phase diagram data is shown, but unrealistic values for the parameters are produced. In the current study, the first assessment of [1995Bra] was preferred due to the more realistic Gibbs energies. The calculated phase diagram is given in Fig. 2.
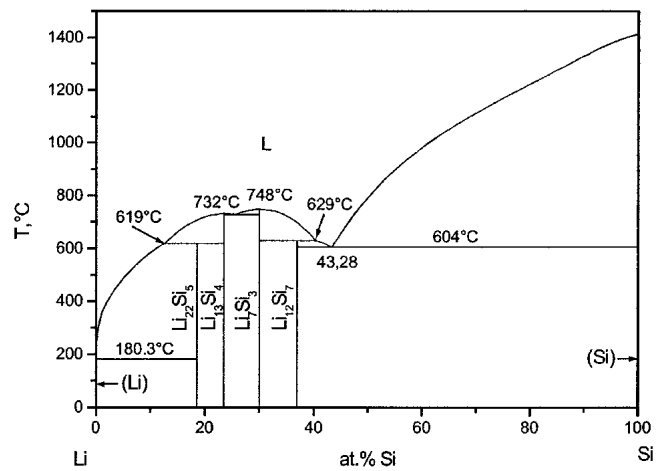
3. Remodeling of the Mg-Si System

A new modeling of the Mg-Si phase diagram was necessary because both of the thermodynamic models presented in recent publications [1997Feu, 2000Yan] exhibited inverted miscibility gaps in of the liquid phase at higher temperatures; these are shown in Fig. 3 and 4. These inverted miscibility gaps are considered artifacts produced by unsuitable temperature dependencies of liquid phase parameters. Such a behavior cannot be accepted, especially for an extrapolation of the binary thermodynamic model into the ternary system at various temperatures.
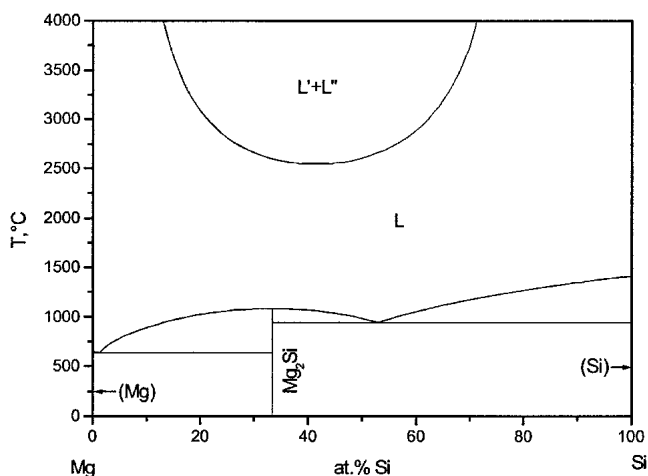
Therefore, the Mg-Si system was remodeled to obtain a phase diagram without an artificial miscibility gap. As a starting point, the assessment of [2000Yan] was used. After correction of the thermodynamic model and reducing the number of parameters the calculated phase diagram still shows a good agreement with the results of experimental investigations (Fig. 5 and 6). No artificial miscibility gap occurs in the liquid even if calculating up to 6000 °C, not shown in Fig. 5. The thermodynamic description of the liquid phase is also in good agreement with experimental thermodynamic data given in Fig. 7, 8, and 9. It should be noted that the slope of the integral enthalpy of mixing at the Mg-rich side in Fig. 8, seemingly not steep enough, should be even less steep, considering the partial enthalpy data of [1997Feu] given in Fig. 9. This inconsistency within the experimental enthalpy data indicate that probably a larger error might be associated with these data, justifying the larger deviation seen in Fig. 8 and 9 and also justifying a more simple thermodynamic description of the liquid phase.

Only one binary phase Mg_2Si forms in the Mg-Si system. It melts congruently and has no detectable homogeneity range. The solid solubility of Mg in (Si) is considered negligible. On the base of x-ray analysis it was shown [1940Kle] that the solubility of Si in (Mg) should be less than 0.1 at.% Si. Raynor [1940Ray] reported the maximum solubility of Si in (Mg) at ≈0.003 at.% Si. This is in good
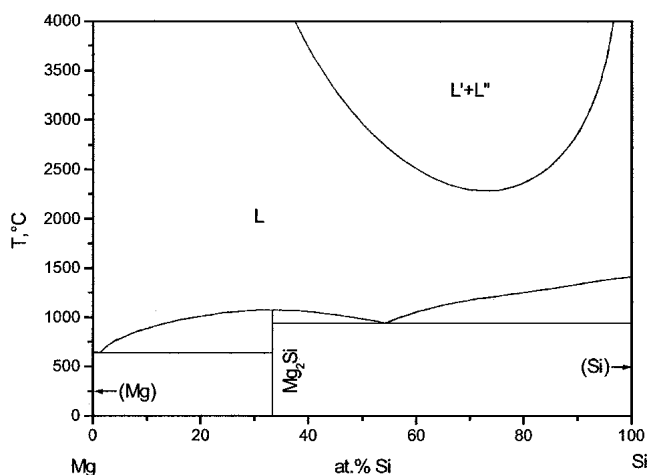
Fig. 3 Calculated phase diagram of the Mg-Si system using parameters of [1997Feu], producing an unrealistic liquid miscibility gap
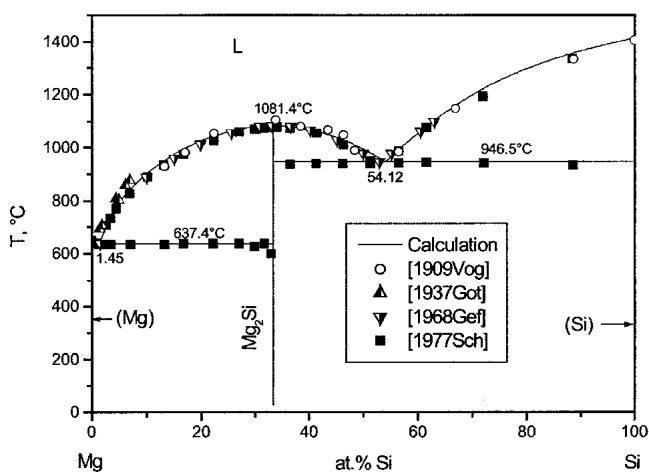

Fig. 5 Calculated phase diagram of the Mg-Si system (this work); the unrealistic inverted liquid miscibility gap at higher temperature does not occur, even if calculating beyond 4000 °C

Fig. 4 Calculated phase diagram of the Mg-Si system using parameters of [2000Yan], producing an unrealistic liquid miscibility gap

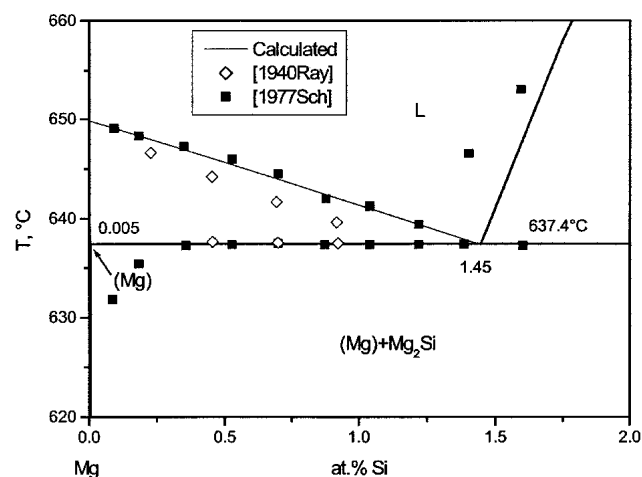**Fig. 6** Calculated Mg-rich side of the Mg-Si phase diagram (this work)

agreement with the results of [1959Yue], who reported a value of 0.0028 at.% Si from a modified zone-melting technique. By contrast, [1977Sch] claimed a larger solubility of ≈0.17 at.% Si in (Mg) on the base of DTA investigation given in Fig. 6, but since these data are in contradiction with the more direct observations, it was not accepted for the modeling. The thermodynamic equations are given in Sec. 6.

4. Ternary Experimental Investigation

To determine a liquidus surface and invariant reactions and to check the ternary phase stability in the Li-Mg-Si system, eight key samples were prepared in the current study, as given in Table 1. The phase analysis was performed by XRD and optical metallography using as-cast

alloys as well as samples after DTA treatment. DTA was used for the polythermal investigation.

Starting materials were Mg chips 99.98 mass%, (Alfa), lithium bulk material 99.9 mass%, (Chemetall, Frankfurt, Germany), and silicon chips 99.9998 mass%, (Wacker, Burghausen, Germany). The elements were weighed and mixed in a glove-box with Ar atmosphere and pressed under a pressure of 100 MPa into small pellets of around 0.5 g. Alloys were prepared from that by levitation melting under purified argon atmosphere. Heating power was controlled carefully to avoid evaporation. Weight loss was found less than 1 mass % after levitation melting.

For XRD analysis, the alloys were powdered in a hand mill and mixed with inert oil to avoid oxidation. Powders could only be produced for Mg-poor samples but not for the highly ductile Mg-rich samples. These samples were polished to obtain a flat surface for x-ray measurements. The x-ray powder diffractometer Siemens D-5000 (Bruker AXS,
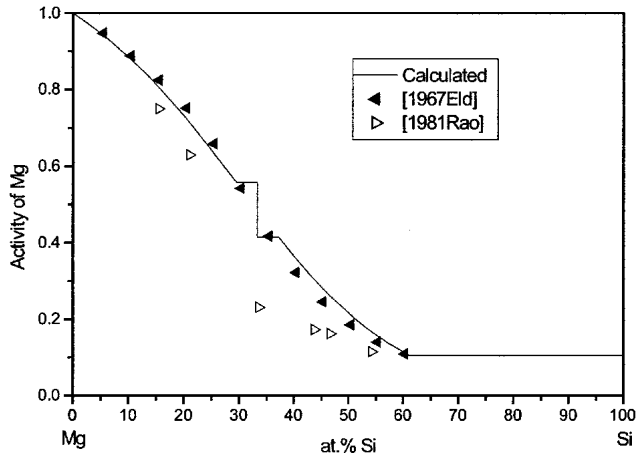
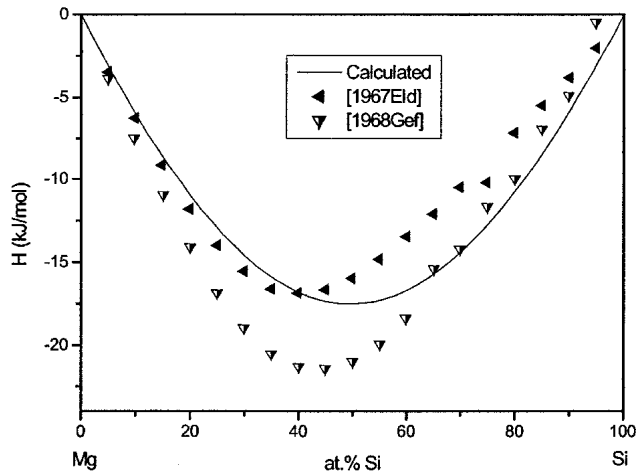**Fig. 7** Activity of Mg in liquid Mg-Si alloy at 1077 °C (referred to Mgl)

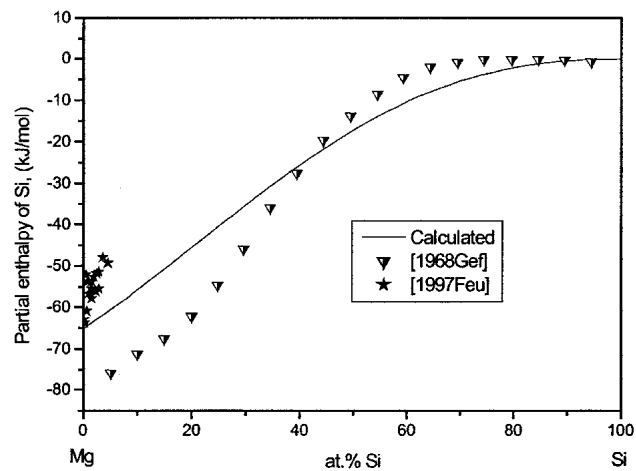**Fig. 8** Enthalpy of the liquid phase at 1077 °C (referred to Mgl and Sil)

Fig. 9 Partial enthalpy of solution of Si in the liquid phase at 1077 °C (referred to Sil)

Table 1   Sample Compositions and Identified Phases

Sample No.	Composition, at.%			Identified Phases After DTA Heat Treatment of 1 K/min (a)
	Li	Mg	Si	
a	53.3	6.7	40	$\tau_1 + [(\tau_3)]$
b	63	16	21	$\tau_2 + [(Li)] + ?$
c	50	25	25	$\tau_3 + [Li_xMg_2Si] + [(Mg)]$
d	25	50	25	$Li_xMg_2Si + [(Mg)] + [\tau_3]$
e	14	58	28	$Li_xMg_2Si + [(Mg)]$
f	20	70	10	$(Mg) + Li_xMg_2Si + \tau_3$
g	10	80	10	$(Mg) + Li_xMg_2Si$
h	8	90	2	$(Mg) + Li_xMg_2Si$

(a) Sequence indicates the amount of phases. Square brackets [] show a very small amount of a phase.

Karlsruhe, Germany) with Co K_α radiation was used for measurements. The routine measurements were performed with a 2θ step of 0.02° and 3 s exposition time in the point. The resultant diffraction patterns were analyzed quantitatively in comparison with simulated x-ray spectra using the program PowderCell 2.1 [1999PC].

Liquidus temperatures and multiphase reactions of the system were investigated by DTA. The samples were sealed under pure argon at 1 bar in specially adapted tantalum containers using electric arc welding. Evaporation and oxidation of the samples was completely avoided with this technique. This procedure enables reproducible DTA signals that cannot be obtained otherwise. As a reference, Al_2O_3 in another sealed Ta crucible was used. The differential thermal analysis was performed using a Netzsch DTA 404 (Netzsch, Selb, Germany). The heating and cooling rates were 5 and 1 K/min. No reactions with the crucibles were observed. For all samples, several heating and cooling runs were performed. After thermal analysis, the alloys were again examined by XRD using the same procedures as described above.

5. Results

5.1 Solid-State Phase Relations

All sample compositions with the identified phases are given in Table 1. Two series of samples were prepared and investigated. The first series of samples, a-d (Fig. 10), was prepared to check the compositions of ternary intermetallic phases reported in literature. The x-ray examination of samples confirmed the formation of the reported phases τ_1, τ_2, and τ_3 as given in Table 2. The second series of samples, e-h, was prepared to investigate in more detail the liquidus surface and the phase relations in the Mg-rich corner.

Three ternary compounds Li_8MgSi_6, $Li_{12}Mg_3Si_4$, and Li_2MgSi were confirmed, denoted as τ_1, τ_2, and τ_3, respectively. The corresponding samples a-c showed traces of additional phases, as presented in Table 1. This supports the finding of [1992Pav] that the ternary phases τ_1, τ_2, and τ_3 are stoichiometric due to inevitable deviations from the nominal composition. The lattice parameters of the ternary phases determined in our study, shown in Table 2, agree perfectly well with published data [1992Pav2]. This also indicates that all the ternary phases have negligible ranges
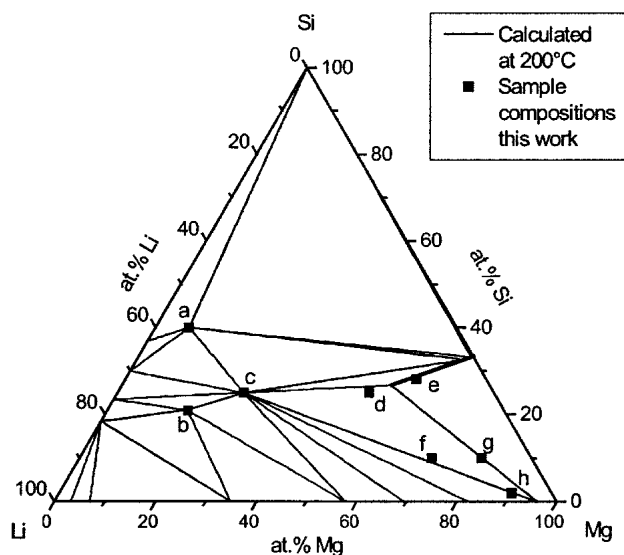
Fig. 10 Calculated isothermal section of the Li-Mg-Si phase diagram at 200 °C; details of the investigated samples are given in Table 1 and details of phase fields are given in Fig. 22.

Fig. 11 Microstructure of the as-cast sample e with the composition $Li_{14}Mg_{58}Si_{28}$ showing the Li_xMg_2Si solid solution (gray) and small amount of Mg (light) in agreement with phase equilibria of Fig. 10

of homogeneity. The $LiMg_2Si$ phase reported by [1992Pav2] was found to be the solid solution of Li in the Mg_2Si phase, denoted as Li_xMg_2Si in the present work. This solid solution was detected by x-ray powder diffraction as well as by metallography. The microstructure of sample e with the composition $Li_{14}Mg_{58}Si_{28}$ ($Li_{0.5}Mg_2Si$) is presented in Fig. 11. It shows an essentially homogeneous phase (Li_xMg_2Si) with trace amounts of (Mg), thus proving the solid solubility of Li_xMg_2Si. This sample would have been located in the center of the two-phase field $LiMg_2Si + Mg_2Si$ assumed by [1992Pav2], which is obviously not present. This ternary solubility of the Mg_2Si binary compound was detected up to ≈23 at.% Li, corresponding to a composition Li_xMg_2Si with $x \approx 0.91$ with an error of probably ±0.05. This limit was estimated using Vegard's law, but since the lattice parameter variation is very small, we could not estimate the limit of solubility more accurately. The crystallographic parameters of the accepted ternary compounds and the Li_xMg_2Si solid solution are presented in Table 2. All the phases detected in samples a-h after the final slow cooling of the DTA cycles using XRD as well as metallography (Table 1) are in perfect agreement with the calculated phase equilibria as discussed later.

5.2 Polythermal Investigation

The first series of thermal analysis measurements was carried out to determine the melting temperature of ternary compounds and the invariant temperatures near the liquidus. Therefore, alloys with the composition of the ternary phases presumed in literature were prepared. All samples were measured several times to verify the results. A preliminary thermodynamic model was then constructed and used to calculate the most important phase equilibria. Since the compositions of samples had small deviations
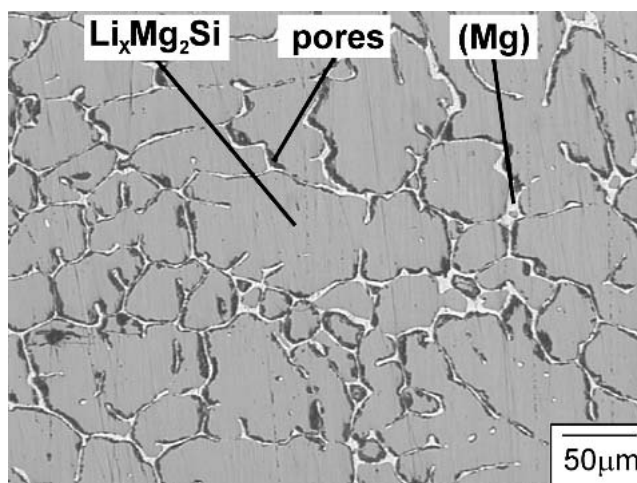
from the stoichiometric compositions of ternary phases, it was possible to detect also some of the phase transformations below the melting points of samples a-c, as given in Table 3.

A second series of sample compositions, d-h, were selected to investigate the Mg-rich corner. Alloy compositions and the DTA results together with the calculated values, and their interpretation are presented in Table 3.

To compare the calculated phase relations in the Li-Mg-Si system with experimental data, several polythermal sections were calculated and are presented in Fig. 12-16. The phase relations in the Mg-rich region are shown in Fig. 15 and 16. The metallographic analysis of as-cast samples g and f, marked in Fig. 15, show a perfect agreement with the calculated phase diagram as demonstrated by their microstructure in Fig. 17 and 18. These samples were "etched" simply by storing for 20 h in dry air, resulting in a darkening of phases with increasing Li-content. This nicely develops the two-phase structure in Fig. 17 and the three-phase structure in Fig. 18.

6. Thermodynamic Modeling

The Gibbs energy function $G_i^{0,\phi}(T) = G_i^\phi(T) - H_i^{SER}$ for the element i ($I = $ Li, Mg, Si) in the ϕ phase [$\phi = $ bcc (Li), hcp (Mg), diamond (Si) or liquid] is described by the equation:

$$G_i^{0,\phi}(T) = a + b \cdot T + c \cdot T \cdot \ln T + d \cdot T^2 + e \cdot T^3 \qquad \text{(Eq 1)}$$
$$+ f \cdot T^{-1} + g \cdot T^7 + h \cdot T^{-9}$$

where H_i^{SER} is the molar enthalpy of the stable element reference (SER) at 298.15 K and 1 bar, and T is the absolute temperature. The Gibbs energy functions for Li, Mg and Si are taken from the SGTE compilation by Dinsdale [1991Din].

Table 2   Accepted Ternary Solid Phases of the Li-Mg-Si System

Phase/ Stability Range	Structure Type	Pearson Symbol	Space Group	Lattice Parameters, nm			Reference
				a	*b*	*c*	
τ_1, Li_8MgSi_6 < 683 °C	Li_8MgSi_6	*mP*96	$P2_1/m$	1.2701	0.4347	1.0507 $\gamma = 107.58°$	1986Nes (a)
τ_2, $Li_{12}Mg_3Si_4$ < 674 °C	$Li_{12}Mg_3Si_4$	*cI*76	$I\bar{4}3d$	1.0688			1992Pav1 1992Pav2 (a)
τ_3, Li_2MgSi < 995 °C	$CuHg_2Ti$	*cF*16	$F\bar{4}3m$	0.637			1992Pav2 (a)
Li_xMg_2Si < 1081 °C $x = 0$ to 0.91	$MnCu_2Al$	*cF*16	$F\bar{4}3m$	0.635 to 0.638			this work

(a) The lattice parameters of the ternary phases were confirmed in this work. The temperature limits were determined in this work both experimentally and by calculation.

The liquid, hexagonal close-packed (hcp) (Mg) and bcc (Li) solution phases are described by the substitutional solution model. For the liquid Mg-Si phase the molar Gibbs energy is expressed by the following equation:

$$
\begin{aligned}
G^{Liq} &= x_{Mg}G_{Mg}^{0,Liq} + x_{Si}G_{Si}^{0,Liq} \\
&+ RT(x_{Mg}\ln x_{Mg} + x_{Si}\ln x_{Si}) \\
&+ x_{Mg}x_{Si}(L_{Mg,Si}^{0,Li} + L_{Mg,Si}^{1,Liq}(x_{Mg} - x_{Si}) \\
&+ L_{Mg,Si}^{2,Liq}(x_{Mg} - x_{Si})^{-2} + \ldots)
\end{aligned} \quad \text{(Eq 2)}
$$

in which R is the gas constant and x_{Mg} and x_{Si} are the molar fractions of Mg and Si. The interaction parameters L^0, L^1, and L^2, may be linearly temperature dependent and are to be optimized. The phases hcp (Mg) and bcc (Li) are described by analogous equations. The ternary data are calculated using a Redlich-Kister/Muggianu-type extrapolation from the binary sets, as given explicitly in [2001Sch], which is reasonable for these chemically not very asymmetric components. No additional ternary interaction parameters were used for any of these phases.

The binary compound Mg_2Si was modeled as a stoichiometric phase referred to the stable elements, and the Gibbs energy (per mol of atoms) is given by

$$
G_{Mg:Si}^{0,Mg_2Si} = \frac{2}{3}G_{Mg}^{0,hcp} + \frac{1}{3}G_{Si}^{0,diamond} + A^{Mg_2Si} + B^{Mb_2Si} \cdot T \quad \text{(Eq 3)}
$$

where the parameters A^{Mg_2Si} and $(-B^{Mg_2Si})$ correspond to the enthalpy and entropy of formation, respectively.

The Li_xMg_2Si phase, extending from the binary Mg_2Si, was modeled as interstitial solid solution, $(Mg)_2(Si)_1(Va,Li)_1$, since the ternary solubility of this compound was experimentally detected to be directed towards pure Li. That means the Mg/Si ratio is constant in that phase. The Gibbs energy (per mol of sites) of this three-sublattice line compound is expressed by

$$
\begin{aligned}
G^{Li_xMg_2Si} &= y_{Va}G_{Mg:Si:Va}^{0,Li_xMg_2Si} + y_{Li}G_{Mg:Si:Li}^{0,Li_xMg_2Si} \\
&+ \frac{1}{4} \cdot R \cdot T(y_{Va} \cdot \ln y_{Va} + y_{Li} \cdot y_{Li})
\end{aligned} \quad \text{(Eq 4)}
$$

in which y_{Va} and y_{Li} are the site fractions of vacancies and Li on the third sublattice. The parameters $G_{Mg:Si}^{0,Li_xMg_2Si}$ (also called compound energies) express the Gibbs energy of the stoichiometric end members of the Li_xMg_2Si phase. Specifically, $G_{Mg:Si:Va}^{0,Li_xMg_2Si} = \frac{3}{4} G_{Mg:Si}^{0,Mg_2Si}$ is the Gibbs energy of binary Mg_2Si (Eq 3). The factor 3/4 accounts for the fact that the phase $(Mg)_2(Si)_1(Va)_1$ has (3 atoms/ 4 sites) in contrast to the phase $(Mg)_2(Si)_1$. The only adjustable parameter, $G_{Mg:Si:Li}^{0,Li_xMg_2Si}$, is that of a fictive end member compound at 25 at.% Li, slightly beyond the solubility limit of ≈23 at.% Li for the Li_xMg_2Si phase. This parameter is sufficient to describe the stability of Li_xMg_2Si, and thus the interactions within the third sublattice are taken to be ideal in the Li_xMg_2Si structure, as given in Eq 4. Ternary solubilities of other binary phases were not found and therefore neglected for the calculation.

The ternary phases τ_1, τ_2, and τ_3 are modeled as stoichiometric compounds, by simply extending Eq 3 to the component Li with the reference state $G_{Li}^{0,bcc}$. No homogeneity ranges were modeled since experimentally no solubilities were observed.

The binary Mg-Si parameters were optimized as detailed in Sec. 3. Using the binary data sets, the ternary Li-Mg-Si phase diagram was first calculated by extrapolation without considering the ternary phases. The solid-state phase relations found in our experimental work and the measured liquidus temperatures were used to determine the linear temperature dependence of the Gibbs energy functions for the ternary phases. The single thermodynamic parameter of the Li_xMg_2Si solution phase was adjusted to meet both the liquidus temperatures measured in the Mg-rich region and the experimentally observed maximum solubility of ≈23 at.% Li. The software Pandat [2002Chen] was used for the calculation.

The comparison between measured and calculated transition temperatures is presented in Table 3 and Fig. 12-16. The calculated ternary invariant reactions are presented in Table 4. The thermodynamic parameters assessed in the present work are given in Table 5. The calculated liquidus surface and three calculated isothermal sections of the

Table 3 DTA Measurements Compared to Thermodynamic Calculations

Sample No.	Heating Rate, K/min	DTA Signals Heating, °C, (a)	DTA Signals Cooling, °C, (a)	Assessed Temperature, °C, (b)	Calculated Temperature, °C	Phase Limits or Invariant Reactions (c)
a	5	m811	o811	811	837	$L/L + \tau_3$
	5	...	o687	688	683	p_1:
	1	...	o689			$L + \tau_3 = \tau_1$
		...	o688			
	5	o684	o661	679	679	U_2:
	1	o679	o664			$L + \tau_3 = \tau_1 + (Si)$
		o678	o664			
b	5	m654	o630	644	674	$? L + \tau_3/L + \tau_3 + \tau_2$
	1	m649	o644			
		m644	o640			
	5	o452	o443	450	455	U_9:
	1	o450	o446			$L + \tau_3 = \tau_2 + (Li)$
		o449	o446			
c	5	m996	o990	996	995	$L/L + \tau_3$
		o948	o947	948	964	$L + \tau_3/L + Li_xMg_2Si + \tau_3$
		m552	o550	551	597	$? U_7$:
		m556	o551			$L + Li_xMg_2Si = \tau_3 + (Mg)$
		m553	o550			
d	5	m1073	o1062	1067	1023	$L/L + Li_xMg_2Si$
	1	m1067	o1064			
		m1070				
	5	o607	o609	608	597	U_7:
	1	o607	o608			$L + Li_xMg_2Si = \tau_3 + (Mg)$
		o607	o608			
		o608	o609			
e	5	o1076	o1076	1076	1060	$L/L + Li_xMg_2Si$
	5	0629	o628	629	629	$L + Li_xMg_2Si/L + Li_xMg_2Si + (Mg)$
f	5	m902	o892	892	877	$L/L + Li_xMg_2Si$
	5	o605	o605	605	597	U_7:
		o602	o603			$L + Li_xMg_2Si = \tau_3 + (Mg)$
		o601	o604			
		o603	o602			
	1	o598	o605			
g	5	m900	o896	899	903	$L/L + Li_xMg_2Si$
	1	m900	o898			
		m899	o899			
	5	o622	o619	621	623	$L + Li_xMg_2Si + (Mg)/$
	1	o619	o621			$Li_xMg_2Si + (Mg)$
		o620	o621			
h	5		o676	674	692	$L/L = Li_xMg_2Si$
	1		o674			
			o672			
	5	o618	o618	617	620	$L + (Mg) + Li_xMg_2Si/$
	1	o613	o617			$(Mg) + Li_xMg_2Si$
		o613	o617			

(a) m, peak maximum; o, peak onset
(b) Estimated DTA error ± 4 K
(c) This interpretation of DTA signals is supported by phase analysis.

Li-Mg-Si phase diagram are presented in Fig. 19-22. In Fig. 19, the primary liquidus field of $Li_{12}Si_7$ is extremely small and located near the binary edge of the phase diagram. Visible on the liquidus surface in that region is merely the primary field of τ_1.

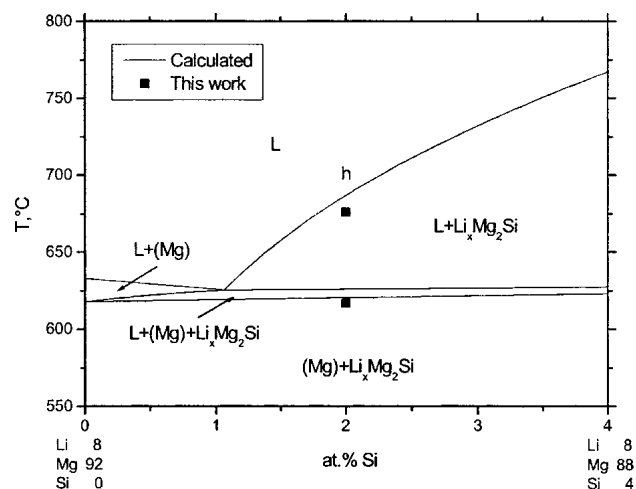## 7. Discussion

The existence of three ternary phases τ_1 (Li_8MgSi_6), τ_2 ($Li_{12}Mg_3Si_4$), and τ_3 (Li_2MgSi) was confirmed during the investigation of the Mg-Li-Si system. Also confirmed was

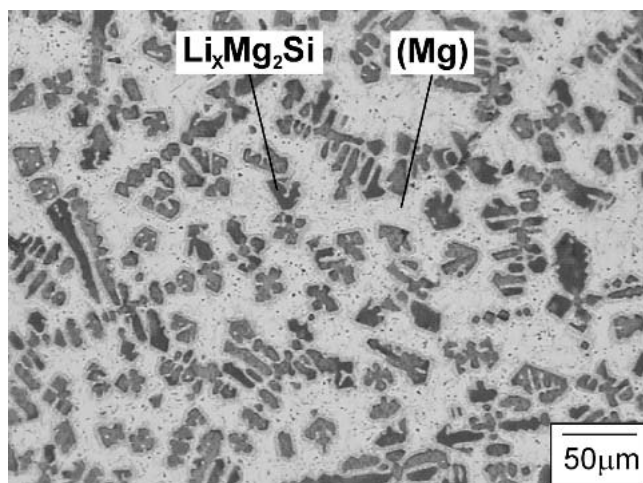**Fig. 12** Calculated polythermal section compared with the DTA measurements for samples a and c; the section deviates slightly from stoichiometric compositions at τ_1 and τ_3.

Fig. 14 Calculated polythermal section compared with the DTA measurements for samples d and e; this section is slightly more Mg-rich than the section Li-Mg$_2$Si.

Fig. 13 Calculated polythermal section compared with the DTA measurements for samples b and c; the section deviates slightly from stoichiometric compositions at τ_2 and τ_3.

Fig. 15 Calculated partial polythermal section of the Li-Mg-Si system at 10 at.% Si compared with the DTA measurements for samples f and g

the previous finding [1992Pav2] that all these phases show negligible ranges of homogeneity.

It was determined by XRD and by metallographic investigation that the LiMg$_2$Si phase reported in [1992Pav2] is approximately the maximum of the solid solution of Li in the binary Mg$_2$Si phase, Li$_x$Mg$_2$Si at $x \approx 0.91 \pm 0.05$. This was also corroborated by DTA measurements, since the liquidus point of sample e (Li$_{14}$Mg$_{58}$Si$_{28}$ or Li$_{0.5}$Mg$_2$Si), is higher than the liquidus point of the sample d (Li$_{25}$Mg$_{50}$Si$_{25}$ or Li$_{1.0}$Mg$_2$Si) (Fig. 14 or Table 3).

The type of solution of Li must be considered to be interstitial due to three reasons: (a) the structure type originally reported [1992Pav2] for LiMg$_2$Si (MnCu$_2$Au) has Li on interstitial sites in Mg$_2$Si; (b) the numerical simulation of the x-ray spectra assuming these Li interstitials in Li$_x$Mg$_2$Si using the program PowderCell 2.1 [1999PC] agrees well

with the experimental spectra but not so well if we assume a substitutional solution; and (c) the direction of solubility range in the ternary is a straight line from Mg$_2$Si towards Li, which means that the ratio Mg/Si is constant, as proven by the microstructure of the Li$_x$Mg$_2$Si ($x = 0.5$) sample presented in Fig. 11, which shows an almost single phase constitution. Therefore a sublattice model (Va,Li)$_1$(Mg)$_2$(Si)$_1$ was selected for that phase. The Li$_x$Mg$_2$Si phase is the only occurrence of ternary solid solubility in a binary phase found in the Li-Mg-Si system.

The solid state equilibria at 200 °C in Fig. 22 are partially also supported by the findings of [1992Pav2], noting that instead of LiMg$_2$Si + Mg$_2$Si only the single phase range Li$_x$Mg$_2$Si exists. Another difference is that τ_3 coexists with Li-Si phases, whereas a conflicting tie line $\tau_2 + \tau_1$ was reported by [1992Pav2]. However, the x-ray spectra of these
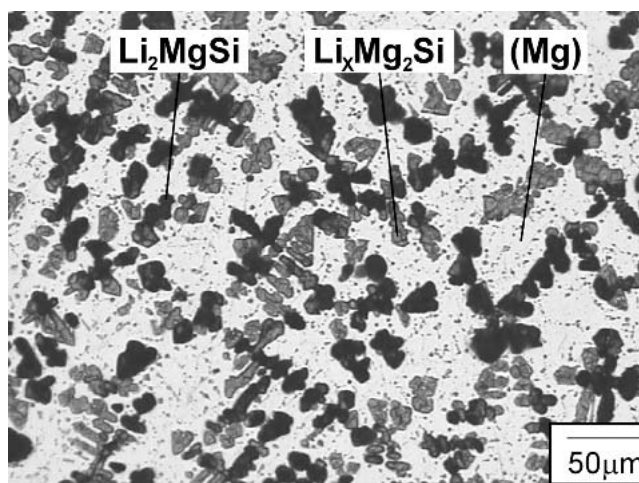
Fig. 16 Calculated partial polythermal section of the Li-Mg-Si system at 8 at.% Li compared with the DTA measurements for sample h

Fig. 18 Microstructure of $Mg_{70}Li_{20}Si_{10}$ as-cast sample f after 20 h in dry air

Fig. 17 Microstructure of $Mg_{80}Li_{10}Si_{10}$ as-cast sample g after 20 h in dry air

Table 4 The Calculated Ternary Invariant Reactions

Reaction	Type	T, °C	Composition of Liquid, (at.%)		
			Li	Mg	Si
$L \leftrightarrow \tau_3$	congruent	995	50	25	25
$L \leftrightarrow \tau_3 + Li_xMg_2Si$	e_1	968	37.26	36.91	25.84
$L \leftrightarrow \tau_3 + Li_7Si_3$	e_2	741	68.85	1.31	29.84
$L \leftrightarrow \tau_3 + Li_{13}Si_4$	e_3	721	74.59	1.91	23.51
$L \leftrightarrow \tau_3 + Li_{13}Si_4 + Li_7Si_3$	E_1	719	73.37	1.58	25.04
$L + Li_xMg_2Si \leftrightarrow (Si) + \tau_3$	U_1	696	49.76	4.96	45.28
$L + \tau_3 \leftrightarrow \tau_1$	p_1	683	54.06	2.04	43.89
$L + \tau_3 \leftrightarrow \tau_1 + (Si)$	U_2	679	51.58	3.45	44.97
$L + \tau_3 \leftrightarrow \tau_2$	p_2	675	79.46	4.40	16.15
$L + \tau_3 \leftrightarrow \tau_2 + Li_{13}Si_4$	U_3	675	79.47	4.27	16.25
$L + \tau_3 \leftrightarrow Li_7Si_3 + \tau_1$	U_4	660	60.64	0.76	38.60
$L + Li_7Si_3 \leftrightarrow \tau_1 + Li_{12}Si_7$	U_5	629	59.52	0.11	40.36
$\tau_3 + (Si) \leftrightarrow \tau_1 + Li_xMg_2Si$	U_6	608	…	…	…
$L \leftrightarrow \tau_1 + Li_{12}Si_7 + (Si)$	E_2	604	56.68	0.03	43.29
$L + Li_xMg_2Si \leftrightarrow \tau_3 + (Mg)$	U_7	597	18.77	80.05	1.18
$L + Li_{13}Si_4 \leftrightarrow \tau_2 + Li_{22}Si_5$	U_8	592	83.84	5.05	11.11
$L \leftrightarrow \tau_3 + (Li)$	e_4	584	27.67	71.19	1.13
$L \leftrightarrow \tau_3 + (Mg) + (Li)$	E_3	583	23.79	75.29	0.91
$L + \tau_3 \leftrightarrow \tau_2 + (Li)$	U_9	455	62.74	36.12	1.13
$L + \tau_2 \leftrightarrow Li_{22}Si_5 + (Li)$	U_{10}	318	80.27	19.21	0.51

phase assemblies are very complex and interpretation may be inconclusive. In addition, the present thermodynamic modeling had shown that a $\tau_2 + \tau_1$ tie line could only be modeled with a much lower stability of τ_3, resulting in a loss of the key equilibrium $\tau_3 + $ (Mg). This $\tau_3 + $ (Mg) equilibrium is firmly established by the XRD analysis of slowly cooled sample f (Table 1), the microstructure of the as-cast sample (Fig. 18), and the secondary DTA effect at U_7 (Fig. 15). It could be even noted from Fig. 15 or the sequence of Fig. 20-22 that in sample f, the amount of τ_3 should increase during cooling from 600 to 200 °C while the amount of Li_xMg_2Si decreases.

Whereas the phase τ_3 in sample f is essentially formed from the liquid phase, this is not the case for sample h. Solidification of h is completed at 620 °C, producing (Mg) + Li_xMg_2Si, the phases actually found in that sample as calculated in Fig. 16. However, the calculated phase equi-

libria indicate a low temperature precipitation of τ_3 at the expense of Li_xMg_2Si in the range 325-219 °C for alloy h. This shift of the three-phase equilibrium (Mg) + Li_xMg_2Si + τ_3 to higher Mg-composition is clearly seen in Fig. 21 and 22. This solid-state transformation is probably too slow to occur in the about 100 min of the DTA experiment in that range. This is the only disagreement of the calculated 200 °C isotherm with the observed phases in any of the samples.

To discuss the DTA results, especially the secondary and higher effects following the primary solidification, Fig. 12 should be more closely examined. The vertical line at 25
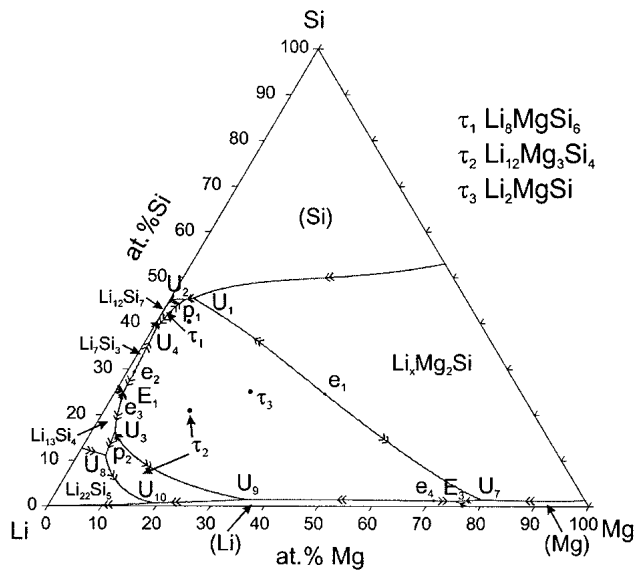
Fig. 19 Li-Mg-Si phase diagram, calculated liquidus surface; invariant reactions and fields of primary crystallization are marked.
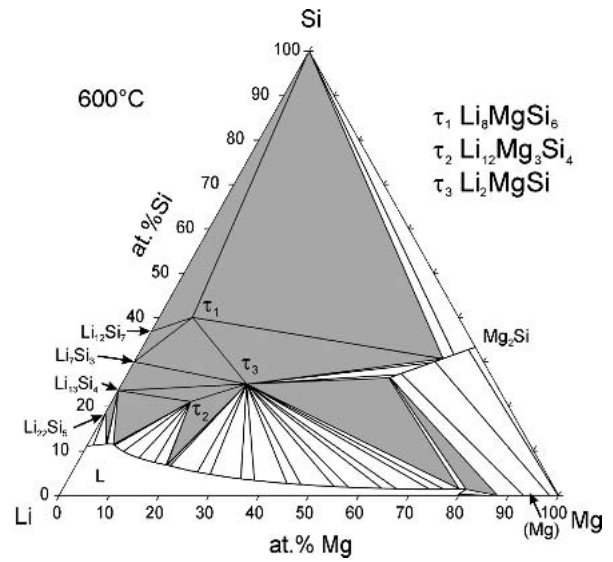

Fig. 20 Calculated isothermal section of Li-Mg-Si phase diagram at 600 °C

Table 5 Thermodynamic Parameters Assessed in the Present Work for the Binary Mg-Si and Ternary Li-Mg-Si Systems in (J/mol of Atoms or Sites), Phase Descriptions bcc = (Li), hcp = (Mg).

$L_{Mg,Si}^{0,Liquid} = -70\,055 + 24.98 \cdot T$

$L_{Mg,Si}^{1,Liquid} = -1300$

$L_{Mg,Si}^{2,Liquid} = +6272$

$L_{Mg,Si}^{0,hcp} = -7148.79 + 0.894 \cdot T$

$G_{Mg:Si:Va}^{0,Li_xMg2Si} = -16\,177.5 + 3.8967 \cdot T + 0.5 \cdot G_{MG}^{0,hcp} + 0.25 \cdot G_{Si}^{0,diamond}$

$G_{Mg:Si:Li}^{0,Li_xMg2Si} = -20\,000 + 0.5 \cdot G_{Mg}^{0,hcp} + 0.25 \cdot G_{Si}^{0,diamond} + 0.25 \cdot G_{Li}^{0,bcc}$

$G_{Li:Mg:Si}^{0,Li2MgSi} = -25\,000 + 0.05 \cdot T + 0.5 \cdot G_{Li}^{0,bcc} + 0.25 \cdot G_{Mg}^{0,hcp} + 0.25 \cdot G_{Si}^{0,diamond}$

$G_{Li:Mg:Si}^{0,Li12Mg3Si4} = -23\,500 + 2.2 \cdot T + 0.631579 \cdot G_{Li}^{0,bcc} + 0.157895 \cdot G_{Mg}^{0,hcp} + 0.210526 \cdot G_{Si}^{0,diamond}$

$G_{Li:Mg:Si}^{0,Li8MgSi6} = -25\,000 + 4.2 \cdot T + 0.533333 \cdot G_{Li}^{0,bcc} + 0.066667 \cdot G_{Mg}^{0,hcp} + 0.4 \cdot G_{Si}^{0,diamond}$

The complete dataset of the ternary system may be obtained on request by sending an e-mail to the corresponding author.

Fig. 21 Calculated isothermal section of Li-Mg-Si phase diagram at 400 °C

at.% Mg, which might be mistaken as the single phase line compound τ_3, is actually composed of densely packed multiphase equilibria. In the upper part it is the L + τ_3 + Li$_x$Mg$_2$Si equilibrium. This is the reason why this line ends at 968 °C and does not touch the liquidus line. This maximum corresponds to e_1 on the eutectic line between τ_3 and Li$_x$Mg$_2$Si, given in Fig. 19. That is, the vertical section in Fig. 12 does not cut exactly through the stoichiometry of τ_3 but at a slightly lower Li-content. This shift also applies to sample c, within 1 mass% weight loss accuracy. This is seen by the second DTA signal at 948 °C (Table 3 and Fig. 12), which in this temperature range could be associated only
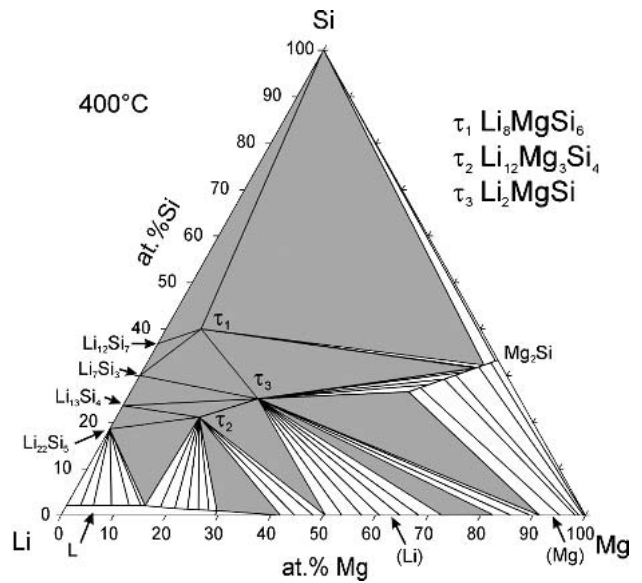
with entering the L + τ_3 + Li$_x$Mg$_2$Si equilibrium, and also by the third signal at 551 °C, where the trace amount of residual liquid solidifies in the probably delayed reaction U7, L + Li$_x$Mg$_2$Si ↔ τ_3 + (Mg), calculated and present in Fig. 12. This interpretation of DTA data is clearly supported by the XRD analysis of sample c, showing mainly τ_3 with traces of Li$_x$Mg$_2$Si and (Mg) (Table 1). This example also shows that a slightly off-stoichiometric sample can convey more information, if linked to a thermodynamic modeling, than a straight τ_3 sample, which would have shown simply the congruent melting point.

The history of sample a, plotted in Fig. 12, is much more straightforward to follow and detailed in Table 3. This
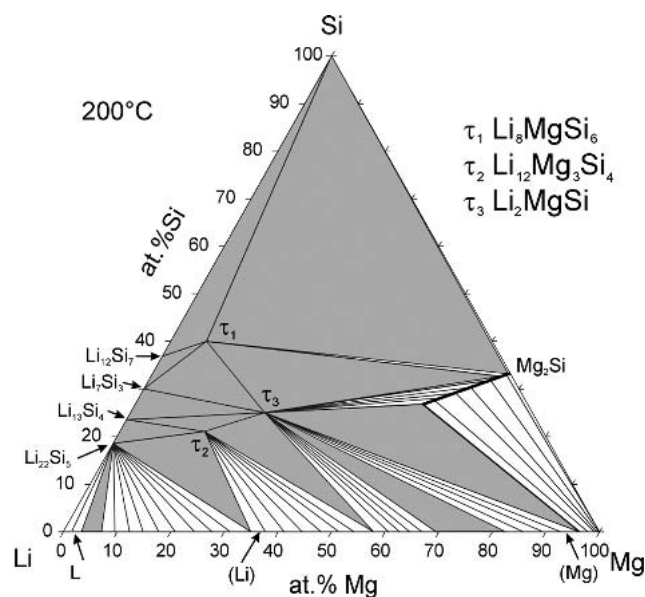
Fig. 22 Calculated isothermal section of Li-Mg-Si phase diagram at 200 °C

sample is composed essentially of τ_1 with traces of τ_3, left over from an incomplete peritectic reaction close to p_1 (Table 1). The minute amount of (Si), expected to be produced in the final transition type reaction U_2, could not be detected by XRD.

Following this detailed example it becomes evident that also for the samples b-h, the interpretation of the DTA signals and the phases identified is supported consistently by the calculated phase equilibria in the vertical sections (Fig. 13-16), the liquidus surface and the isothermal sections in Fig. 19-22. It would be virtually impossible to understand quantitatively and consistently the solidification and melting behavior of these samples without the calculated phase diagram. This is also important for the practical application to a preparation of the intermetallic phases with high purity. To control trace amounts of foreign phases, the entire ternary phase diagram has to be known.

The slight off-stoichiometry is also the reason why the pack of vertical lines in Fig. 13 at 25 at.% Mg does not extend up to the congruent melting point of τ_3. Again, entering the $L + Li_xMg_2Si + \tau_3$ field results in the second thermal effect experienced by sample c.

The attempts to model the Li_xMg_2Si solution phase according to the rather high melting point of sample d in Fig. 14 produced a too-high and too-large liquidus surface of Li_xMg_2Si and unreliable phase transformations and solid-state equilibria in the Mg-rich corner. It was considered more important to meet the liquidus points in the Mg-rich region in Fig. 15 and 16, where the additional agreement with the secondary DTA effects provides an important check of the overall consistency of the data.

Figure 14 displays a sharp corner in the phase boundary $L + Li_xMg_2Si$ / $L + Li_xMg_2Si + \tau_3$ around 953 °C and 54 at.% Mg. One might expect a solidus line of Li_xMg_2Si extending from around that point to the melting point of pure Mg_2Si. However, this line exists only on the exact stoichi-

ometric section Li-Mg_2Si. The section in Fig. 14 ends at the slightly more Mg-rich point $Mg_{66.7}Si_{33.3}$, and therefore no solidus line can exist. The $L + Li_xMg_2Si$ field exists well below 953 °C with a very small amount of residual liquid until the extremely narrow $L + Li_xMg_2Si + (Mg)$ equilibrium, where the second DTA effect of sample e occurs, and the small amount of (Mg) precipitates, seen in Fig. 11 and also by XRD.

It is interesting to note that the $L + Li_xMg_2Si$ / $L + Li_xMg_2Si + \tau_3$ phase boundary below the sharp corner moves backwards to lower Mg-content. That means that the reaction type of solidification must change gradually from eutectic, $L \rightarrow Li_xMg_2Si + \tau_3$, to peritectic, $L + \tau_3 \rightarrow Li_xMg_2Si$, in that region. This is verified by the solidification path of an alloy on the section in Fig. 14, just a little left of that corner. Let us follow the alloy with 53.3 at.% Mg, 20.09 at.% Li, and 26.61 at.% Si, that enters the three phase field at 959 °C and leaves it again at 843 °C. At both ends the amount of τ_3 is zero, so it must have a maximum in between. Indeed, the calculation shows this maximum at 937 °C with a molar phase fraction of 0.013 for τ_3. It also shows the monotonic growth of Li_xMg_2Si and consumption of L during cooling from 959 to 843 °C. Thus, if we place the consumed phases to the left and the growing phases to the right of the arrow, we have the reactions

$L \rightarrow Li_xMg_2Si + \tau_3$, 959 to 937 °C, and
$L + \tau_3 \rightarrow Li_xMg_2Si$, 937 to 843 °C
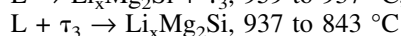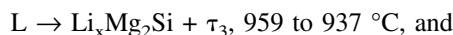
for the selected alloy. The solidification continues with $L \rightarrow Li_xMg_2Si$, 843-606 °C.

This is a nice real example of the intricacies involved in gradually changing reaction types, discussed in general terms by Hillert [1998Hil]. Specifically, it is not decisive to look if an extended line of a tangent to the monovariant line e_1 in Fig. 19 crosses between the compositions of τ_3 and Li_xMg_2Si. The transition for the alloy with 53.3 at.% Mg discussed above occurs at 937 °C with a liquid composition of 50 at.% Mg along line e_1. Here, the classic textbook criterion of the tangent gives the wrong impression of an ongoing eutectic type reaction e_1. The transition point also depends on alloy composition. For sample d in Fig. 14 with 50 at.% Mg, the maximum of τ_3 production occurs at 758 °C, corresponding to a liquid composition of 72 at.% Mg along line e_1 in Fig. 19. Again, at this point, the plotted tangent crosses between the compositions of τ_3 and Li_xMg_2Si, giving no indication for the actually changing reaction type.

The reason for the failure of the classic tangent criterion is that the Li_xMg_2Si solid composition also moves. Therefore, the eutectic/peritectic transition also depends on the overall alloy composition in the three-phase field and may occur at different temperatures. The only practical way to detect the transition is to calculate the solidification path and phase amounts for a given alloy. Only if both solid phase compositions are fixed does the classic tangent criterion hold true for this transition.

8. Conclusion

The thermodynamic parameters for the binary Mg-Si subsystem were remodeled to avoid an artificial inverted liquid miscibility gap at higher temperature. This was necessary to obtain data that could be reliably extrapolated to various temperatures and into the ternary system.

Using XRD, optical metallography, and DTA three ternary phases were confirmed: τ_1 (Li_8MgSi_6), τ_2 ($Li_{12}Mg_3Si_4$), and τ_3 (Li_2MgSi). The $LiMg_2Si$ phase reported in [1992Pav2] is not a separate phase but the interstitial solid solution of Li in the binary Mg_2Si phase, Li_xMg_2Si at the maximum $x \approx 0.91 \pm 0.05$. Ternary liquidus data and phase transformations were also measured.

A thermodynamic assessment of the ternary Li-Mg-Si system was worked out in parallel to the experimental study and used to select the relatively small number of our key experiments. The final consistent thermodynamic model is well supported by the present experimental data and the published phase relations at 200 °C [1992Pav2]. The three solution phases liquid, (Mg) and (Li) are sufficiently described by extrapolations of their binary thermodynamic models without ternary interactions. Only the three ternary phases and the Li_xMg_2Si solution had to be modeled.

Solidification and phase transformations occurring in samples slightly off the stoichiometry of the ternary intermetallic phases are rather intricate. It is demonstrated that this intricate behavior can be quantitatively understood using a number of calculated ternary phase diagram sections and invariant reactions. This knowledge may be also important in the processing of these intermetallic phases and the control of trace amounts of foreign phases.

It is also shown that the gradual change from eutectic, $L \rightarrow Li_xMg_2Si + \tau_3$, to peritectic, $L + \tau_3 \rightarrow Li_xMg_2Si$, monovariant reaction type transition depends on the overall alloy composition in the three-phase field and may occur at different temperatures. The classic tangent criterion fails, since not only the liquid but also the Li_xMg_2Si solid composition moves with temperature.

If lithium is added to Mg alloys containing small amounts of Si, it dissolves at a higher fraction in the Mg_2Si phase compared with the (Mg) matrix. At higher lithium addition the ternary phase τ_3 (Li_2MgSi) starts forming.

Acknowledgment

References

1909Vog: R. Vogel: *Z. Anorg. Chem.*, 1909, *61,* pp. 46-63.

1937Got: M. Goto, M. Nito, and H. Asada: *Rept.Aeronaut., Research Inst. Tokyo Univ.*, 1937, *12,* pp. 163-318.

1940Kle: W. Klemm and H. Westlinning: *Z. Anorg. Chem.*, 1940, *245,* pp. 365-80.

1940Ray: G.V. Raynor: *J. Inst. Met.*, 1940, *66,* pp. 403-26.

1959Yue: A.S. Yue, *Trans. TMS-AIME*, 1959, *215,* pp. 870-71.

1967Eld: J.M. Eldridge, E. Miller, and K.L. Komarek: *Trans. TMS-AIME,* 1967, *239,* pp. 775-81.

1968Gef: R. Geffken and E. Miller: *Trans.TMS-AIME*, 1968, *242,* pp. 2323-28.

1977Sch: E. Schürmann, A. Fischer: "Teil 2. Zweistoffsystem Magnesium-Silicium," *Giessereiforschung*, 1977, *29,* 111-13 (in German).

1981Rao: Y.K. Rao and G.R. Belton, *Chemical Metallurgy—A Tribute to Carl Wagner,* N.A. Gokcen, ed., TMS-AIME, Warrendale, PA, 1981, pp. 75-96.

1986Nes: R. Nesper, J. Curda, and H.G. von Schnering: "Li_8MgSi_6 a Novel Zintl Compound Containing Quasi- Atomic Si_5 Rings," *J Solid State Chem.,* 1986, *62,* pp. 199-206.

1990Sau: N. Saunders: "A Review and Thermodynamic Assessment of the Al-Mg and Mg-Li System," *Calphad*, 1990,*14*(1), pp. 61-70.

1991Din: A.T. Dinsdale: "Thermochemical Data of the Elements," *Calphad*, 1991, *15,* pp. 317-425.

1992Pav1: V.V. Pavlyuk and O.I. Bodak: "The Crystal Structure of the $Li_{12}Mg_3Si_4$ and $Li_{12}Al_3Si_4$ Compounds," *Neorg. Mater.,* 1992, *28,* pp. 988-90 (in Russian).

1992Pav2: V.V. Pavlyuk, O.I. Bodak, and G.S. Dmytriv: "Interaction of the Components in the Li-{Mg,Al}-Si Systems," *Ukr. Khim. Zh.,* 1992, *58,* pp. 735-37 (in Russian).

1995Bra: M.H. Braga, L.F. Malheiros, and I. Ansara: "Thermodynamic Assessment of the Li-Si System,"*J. Phase Equilibria,* 1995, *16,* pp. 324-30.

1997Feu: H. Feufel, T. Gödecke, H.L. Lukas, and F. Sommer: "Investigation of the Al-Mg-Si System by Experiments and Thermodynamic Calculations," *J. Alloys Compd.*, 1997, *247,* pp. 31-42.

1998Hil: M. Hillert, *Phase Equilibria, Phase Diagrams and Phase Transformations—Their Thermodynamic Basis,* Cambridge University Press, Cambridge, UK, 1998.

1998Sau: N. Saunders: "System Li-Mg" in *COST507— Thermochemical Database for Light Metal Alloys,* I. Ansara,, A.T. Dinsdale, and M.H. Rand, ed., European Commission, Luxembourg, EUR 18499 EN, 1998, pp. 210-12.

1999PC: W. Kraus and G. Nolze, *PowderCell* for Windows, Version 2.1, 15.02.1999, Federal Institute for Materials Research and Testing, BAM, Berlin, Germany, 1999.

2000Yan: X-Y. Yan, F. Zhang, and Y.A. Chang: "A Thermodynamic Analysis of the Mg-Si System," *J. Phase Eq.*, 2000, *214,* pp. 379-84.

2001Sch: R. Schmid-Fetzer and J. Gröbner: "Focused Development of Magnesium Alloys Using the Calphad Approach," *Adv. Eng. Mater.,* 2001, *3,* pp. 947-61.

2002Chen: S-L. Chen, S. Daniel, F. Zhang, Y.A. Chang, X-Y. Yan, F-Y. Xie, R. Schmid-Fetzer, and W.A. Oates: "The Pandat Software Package and its Applications," *Calphad*, 2002, *26,* pp. 175-88.

2003Pan: Anon., *WinPhad 4.0-H,* Phase Diagram Calculation Engine for Multicomponent Systems, CompuTherm LLC, 437 S. Yellowstone Dr., Suite 217, Madison, WI, 2000.